Journal of Heat Transfer

Technical Brief

Pool Boiling Experiments on Multiwalled Carbon Nanotube (MWCNT) Forests

Hee Seok Ahn

Nipun Sinha

Mechanical Engineering Department,
Texas A&M University,
College Station, TX 77843-3123

Mei Zhang
NanoTech Institute and Department of Chemistry,
University of Texas at Dallas,
Richardson, TX 75083

Debjyoti Banerjee
Mechanical Engineering Department,
Texas A&M University,
College Station, TX 77843-3123

Shaoli Fang

Ray H. Baughman

NanoTech Institute and Department of Chemistry,
University of Texas at Dallas,
Richardson, TX 75083

In this study, two silicon wafer substrates were coated with vertically aligned multiwalled carbon nanotubes (MWCNT) "forests" and were used for pool boiling studies. The MWCNT forests (9 and 25 μm in height) were synthesized on the silicon wafer substrates using chemical vapor deposition (CVD) process. The substrates were clamped on a cylindrical copper block with embedded cartridge heaters. The heat flux was measured using sheathed K-type thermocouples, which were placed inside the cylindrical copper block. Pool boiling experiments using refrigerant PF-5060 as the working liquid were conducted to obtain the pool "boiling curve." The experiments were conducted in nucleate and film boiling regimes to investigate the effect of MWCNT height on pool boiling performance. Reference (control) experiments were also performed with an atomically smooth bare silicon wafer (without MWCNT coating). The results show that the MWCNT forests enhanced critical heat flux (CHF) by 25–28 % compared to control experiments. For the film boiling regime, Type-B MWCNT (25 μm in height) yields 57% higher heat flux at Leidenfrost point (film boiling regime) compared to control experiments. However, for the Type-A MWCNT (9 μm in height) the film boiling heat flux values are nearly identical to the values obtained for the control experiments performed on bare silicon.
[DOI: 10.1115/1.2349511]

Keywords: carbon nanotube, CNT, pool boiling, critical heat flux, Leidenfrost boiling, silicon wafer

Introduction

Boiling is the most efficient mode of heat transfer. Hence, it is considered an attractive option for the emerging thermal management schemes. In addition, perturbing various transport mechanisms in boiling is important for energy conversion devices, insulation schemes for cryogenic systems, energy storage, materials processing, and futuristic applications (e.g., ablation cooling for high-speed civil transport). Many researchers reported the enhancement of boiling heat transfer by using novel materials or structures. Ramaswamy et al. [1] conducted experiments by employing enhanced structures consisting of six layers of copper plates with rectangular channels cut on either side of the plates. The combined effect of the system pressure and liquid subcooling on the boiling performance of the enhanced structure was studied in these experiments. The authors reported that boiling heat flux increased on the enhanced structures. The combined effects of subcooling and system pressure were also found to augment the boiling heat flux on the enhanced structures. Mudawar and Anderson [2] performed pool-boiling experiments using multiple levels of enhanced surfaces on a pin fin and obtained critical heat flux (CHF) of 105.4 W/cm^2 and 159.3 W/cm^2 using FC-72 as a working fluid under saturated and subcooled conditions (for 35°C liquid subcooling), respectively. Coursey et al. [3] used graphite foams for pool-boiling experiments. The effects of chamber pressure, liquid level, and working fluid on nucleate boiling were reported in this study. The thermal conductivity of the component graphite ligaments in the foams was reported to be five times higher than for copper. The thermal diffusivity of bulk graphite foam was reported to be four times that of aluminum due to the higher thermal conductivity and lower density. The authors reported that using graphite foams as an evaporator in a thermosiphon enhanced cooling for a fixed wall temperature, especially at lower chamber pressure. The enhanced cooling at lower pressure can be attributed to a decrease in saturation temperature, which corresponds to an increase in wall superheat (for a fixed wall temperature).

After discovery of carbon nanotubes (CNT) in 1991 by Iijama [4], there has been a growing interest for various applications of CNT. CNT have very broad range of thermal, electrical, and struc-

Contributed by the Heat Transfer Division of ASME for publication in the JOURNAL OF HEAT TRANSFER. Manuscript received November 8, 2005; final manuscript received May 29, 2006. Review conducted by Ramendra P. Roy.

Table 1 Thermo-physical properties of PF-5060 at atmospheric pressure [6]

Property	Liquid	Vapor
Density, kg/m^3	1610.68	12.52
Kinematic viscosity, kg/m^3	2.78×10^{-7}	1.15×10^{-6}
Prandtl number	9.8	0.81
Specific heat, J/kg-K	1132.62	651
Thermal conductivity, W/m-K	0.0539	0.0124
Surface tension, N/m	8.448×10^{-3}	
Latent heat of vaporization, J/kg	85034.34	

tural properties that can be tailored to various molecular structural types (length, diameter, and orientation). According to Berber et al. [5], the thermal conductivity value of CNT is 6600 W/m K (around 17 times higher than that of copper) at room temperature and drops drastically to 3000 W/m K (around eight times higher than that of copper) at 400 K.

In this study, the effect of nanostructured surfaces on pool boiling was studied for nucleate and film boiling regimes. The aim of this study was to explore the physics of the transport mechanisms during pool boiling on nanostructured surfaces. The ultimate goal is to understand the transport mechanisms on the nanoscale and therefore prepare the foundations for developing new methods for augmenting heat transfer.

The nanostructured surfaces were realized by the synthesis of vertically aligned multiwalled carbon nanotubes (MWCNT) on atomically smooth silicon wafer substrates using chemical vapor deposition (CVD) process. An experimental apparatus was built for pool boiling studies that consisted of a viewing chamber containing a heater unit. The silicon wafer substrate with either the nanostructured surface or the atomically smooth bare surface was clamped on the heater unit and pool boiling experiments were performed on these surfaces. The property values of the working fluid (PF-5060, manufactured by 3M Co.) are listed in Table 1 [6].

Experimental Apparatus

The experimental apparatus used in this study consists of: (i) a viewing chamber, which is used to house; (ii) a heater unit; and (iii) a silicon substrate clamped on top of the heater unit. The voltage signals from the thermocouples embedded in the heater unit were recorded using a computer-controlled high-speed data acquisition system. Figure 1 shows the schematic diagram of the experimental setup.

Heater Unit. A heater unit was mounted inside the viewing chamber. The heater unit was fabricated by enclosing the cylindrical copper block (8.89 cm dia) inside an annular steel jacket. The annular steel jacket was used to prevent any boiling from occurring on the sides of the copper block. A silicon wafer was placed on top of the copper block and clamped with an annular steel disk. A Pyrex® wafer was placed between the silicon wafer and the copper block to minimize the electrical noise from heaters. Five cartridge heaters were placed in the copper block (three of 500 W rating and two of 300 W rating, manufactured by Watlow Inc.). Twelve K-type thermocouples were flush mounted inside holes drilled at different depths and radial locations along the side of the copper block. One thermocouple was placed in the liquid PF-5060 to ensure the bulk liquid was maintained at saturation temperature.

Synthesis and Growth of MWCNT on Silicon. MWCNT forests were grown on the silicon wafer using chemical vapor deposition (CVD) techniques. The MWCNT structures were uniform in height (Fig. 2(*a*)). Two different heights of MWCNT forests were used in the experiments: with heights of 9 and 25 μm, respectively. The heights of MWCNT were selected so that one is smaller and the other is greater than the dynamic value of the minimum vapor film thickness in film boiling. According to numerical and experimental results by Banerjee and Dhir [7,8] and Banerjee et al. [9], the dynamic values of the minimum vapor film thickness in film boiling of PF-5060 is $\sim$15–20 μm. Figure 2 shows the SEM images of the silicon wafer substrates containing MWCNT forests. Typically, the vertically aligned MWCNT "for-

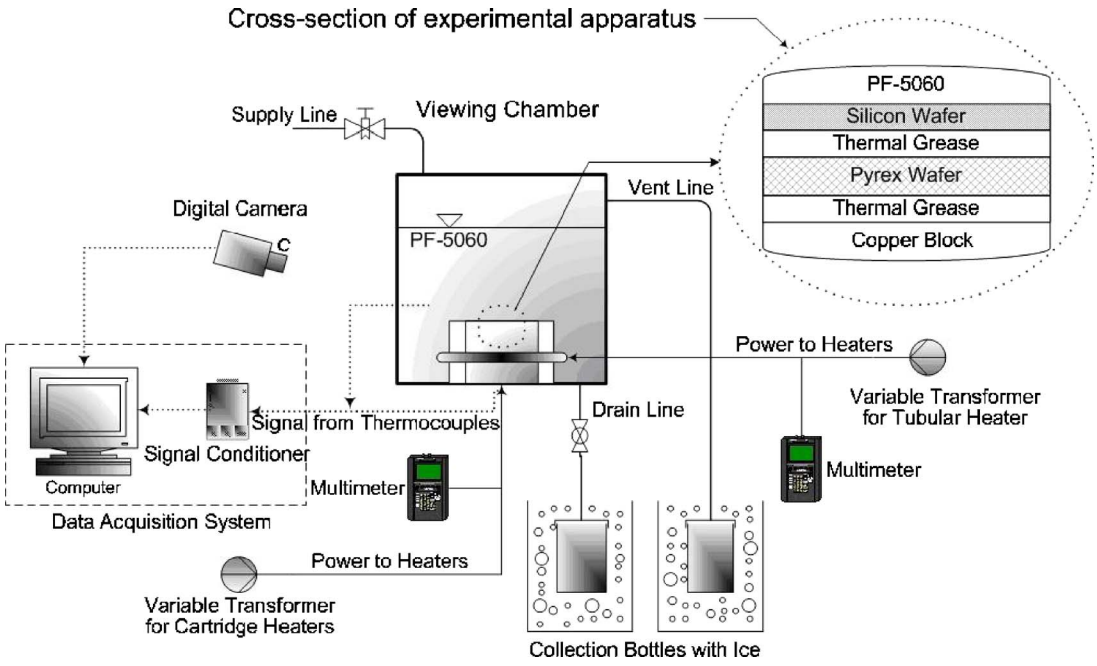

Fig. 1 Schematic diagram of experimental apparatus consisting of: (1) viewing chamber, (2) heater apparatus, and (3) silicon wafer surface with multiwalled carbon nanotube (MWCNT) forests

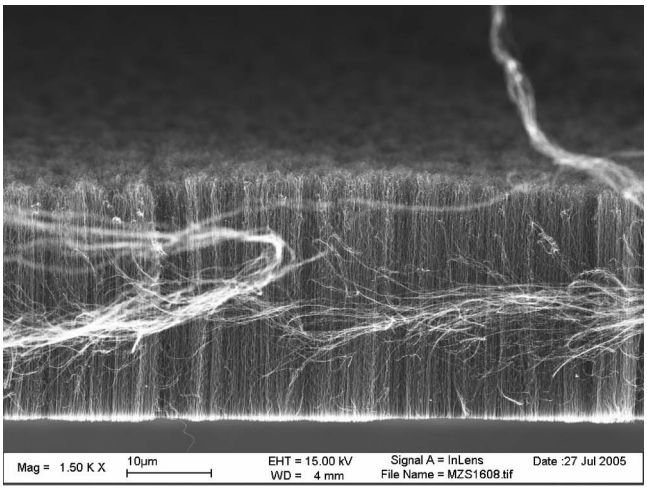

(*a*)

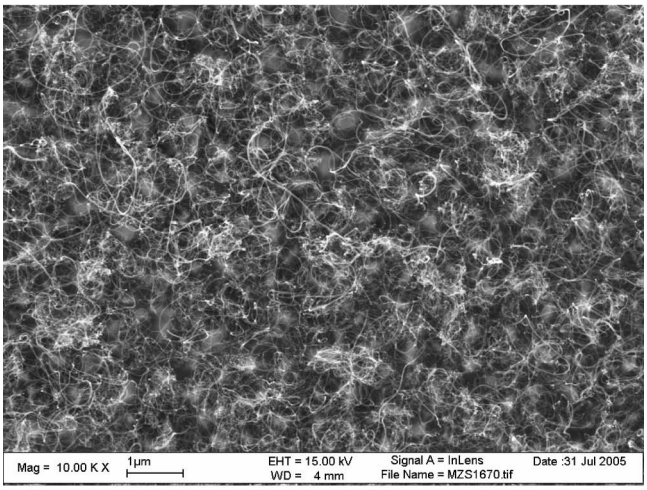

(*b*)

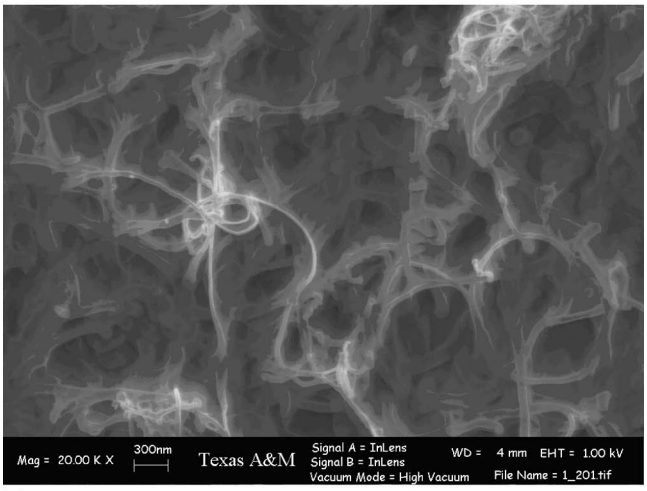

(*c*)

Fig. 2 SEM image of type-B MWCNT (25 μm in height) synthesized on silicon substrate: (*a*) side view before experiment, (*b*) top view before experiment, and (*c*) top view after experiment

ests" are synthesized using the CVD process—by flowing 5 mol.% C_2H_2 at 580 sccm (standard cubic centimeters per minute) in He at atmospheric pressure in a quartz tube maintained at 680°C. To obtain MWCNT of desired height, the synthesis time can range from a few seconds to ~10–20 min since the growth rates of the MWCNT are ~1–2 μm/min. Prior to performing CVD synthesis of MWCNT an iron film of 5 nm thickness was deposited on the silicon wafer by electron beam evaporation to serve as a catalyst. Earlier investigations [10] using SEM and thermal gravimetric measurements indicated that the purity of the synthesis process was very high (~96–98 % Carbon in the form of MWCNT) with 2–4 % Fe and amorphous carbon. No carbon particles were observed in these tests. The diameter of the vertically aligned MWCNT varied from ~8–16 nm. The CVD process results in nucleation and growth of the MWCNT on a random pitch of ~8–16 nm on the silicon substrate, resulting in a high surface coverage and high surface density of the nanotubes. Therefore, the surface density of the MWCNT was not controlled in this nanosynthesis process. Details about the CVD process for synthesis and growth of MWCNT forests are described in [10].

Experimental Procedure

Pool boiling experiments were conducted under steady-state conditions. The voltage input to the heaters was adjusted by a variac and increased from 13 V to 35 V in increments of 3–5 V for obtaining the nucleate boiling segment of the boiling curve until the maximum heat flux condition (critical heat flux (CHF)) was reached. Incrementing the input voltage by ~0.5 V beyond CHF resulted in transition boiling and rapid increase in temperature of the heater apparatus. The input voltage was then reduced progressively until stable film boiling was obtained. During film boiling, the voltage was reduced in steps of ~0.5–2 V until transition boiling was obtained. This procedure was used to estimate the "hysteresis" in the boiling curve. Typically, each voltage setting required 2–3 h to obtain steady state and required a total time of ~24–36 h to conduct each experiment.

Before starting each experiment, the liquid pool was boiled using a tubular heater that was installed around the steel jacket. This was performed to remove any dissolved gases in PF-5060 and to heat the side-walls of the viewing chamber so that rapid convergence to steady-state conditions could be obtained. During the experiments, especially at lower superheats, the input power to the tubular heater was adjusted by a variac in order to maintain the liquid temperature in the pool at the saturation temperature of PF-5060 (56°C). The working liquid was periodically replenished into the pool to maintain the liquid level within a height of 3.2–4.5 cm above the boiling surface during the experiments. Typically, the liquid level was replenished after recording each steady-state data and required ~2–3 h of waiting time for obtaining steady-state temperature conditions after each replenishment.

After steady-state conditions were reached, the temperatures from the wire-bead K-type thermocouples (embedded in the copper block) were recorded with a computer-controlled high-speed data acquisition system. The data acquisition system consisted of NI SCXI-1102C Analog MUX, and PCI-6251 DAQ board with Pentium-4 3.2 GHz computer, and controlled by a software program coded using LABVIEW 7.1 (Manufactured by National Instruments). To ensure that the working liquid was maintained at saturation temperature, the temperature from a thermocouple submerged in the liquid pool was continuously recorded and monitored.

Data Reduction

The heat flux [in watts per meters squared] was evaluated from the gradient of the temperature profiles in the copper block

$$q'' = -k\frac{\Delta T}{\Delta x} \tag{1}$$

where k is the thermal conductivity of the copper block (watts/meter Kelvin), ΔT is the temperature difference between two thermocouples lying in the same vertical plane [in degrees Celsius], and Δx is the distance (in meters) between the thermocouples.

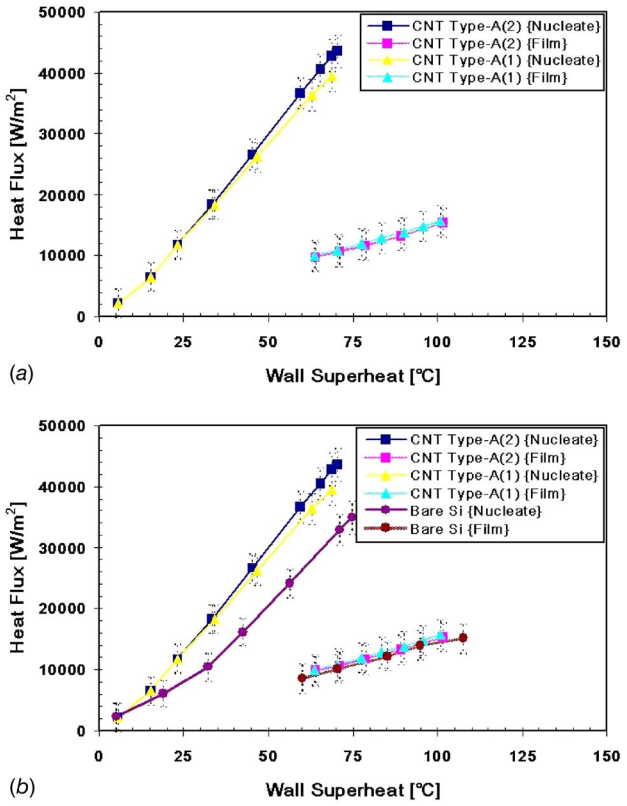

Fig. 3 Saturated pool boiling curve for PF-5060 on type-A MWCNT (9 μm in height) synthesized on silicon wafer. Saturation temperature of PF-5060=56°C. (*a*) Pool boiling curve for PF-5060 on type-A MWCNT. (*b*) Comparison of pool boiling curve of type-A MWCNT with bare silicon. (the numbers in parenthesis denote the experimental run.)

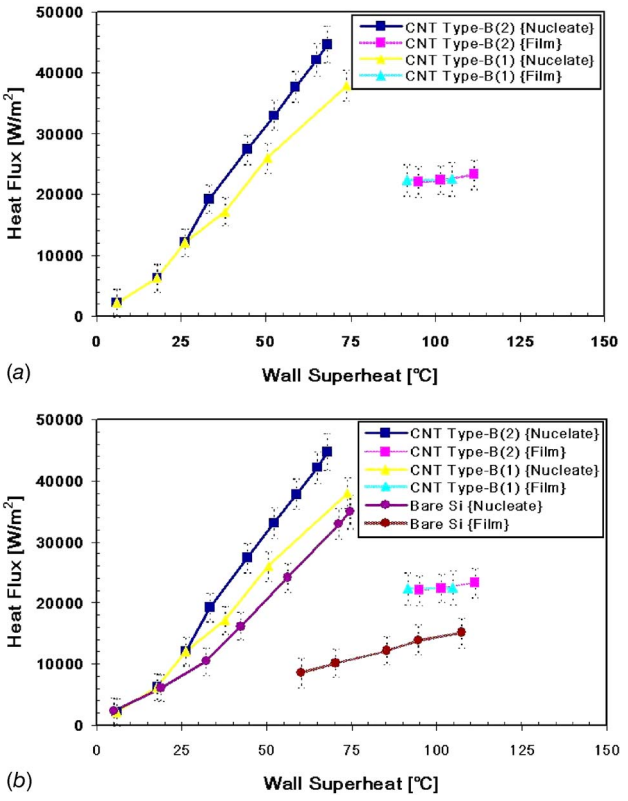

Fig. 4 Saturated pool boiling curve for PF-5060 on type-B MWCNT forests (25 μm in height) synthesized on silicon wafer. The saturation temperature of PF-5060=56°C. (*a*) Pool boiling curve for PF-5060 on type-B MWCNT. (*b*) Comparison of pool boiling curve for type-B MWCNT with bare silicon (the numbers in parenthesis denote the experimental run).

In this experiment, the wall temperatures were calculated by utilizing thermal resistance values obtained from prior temperature measurements using surface micromachined thin film thermocouple (TFT) on the silicon wafer [11]. From these experiments [11], the correlation of the thermal resistance (R_t (watts/degrees Kelvin)) between the silicon wafer surface (at the boiling surface) and top of the copper block in nucleate and film boiling regime was

$$R_t = (-4 \times 10^{-4})T_c + 0.2302 \text{ (nucleate boiling)};$$

$$R_t = 0.1037 \text{ (film boiling)} \quad (2)$$

where T_c is the temperature at top surface of the copper block (degrees Celsius) obtained from the embedded thermocouples.

The wall temperature was calculated using Eq. (3).

$$T_w = T_c - q'' A_w R_t \quad (3)$$

where, T_w is the wall temperature (degrees celsius), A_w is the boiling area (meters squared). The experimental uncertainties for q'' (and, therefore, R_t) in these experiments was ±15.5% and ±20.5% in nucleate and film boiling, respectively [11].

The uncertainty of the heat flux and the heat transfer coefficient in boiling were calculated using Kline and McClintock method [12] as follows:

$$\frac{\omega_{q''}}{q''} = \sqrt{\left(\frac{\omega_k}{k}\right)^2 + \left(\frac{\omega_{\Delta T}}{\Delta T}\right)^2 + \left(\frac{\omega_{\Delta x}}{\Delta x}\right)^2} \quad (4)$$

where ω is the statistical uncertainty value for each variable.

The uncertainty in determination of the vertical distance between two thermocouples embedded in the copper block was estimated to be ±3.0%, which was determined by the machining accuracy. The uncertainty of the thermal conductivity of the copper block was assumed to be ±1.0% based on thermophysical property table [13]. The uncertainty in determination of the temperature difference was estimated from a number of sources. Since 16 bit precision was used in the data acquisition hardware the absolute precision was ±0.005°C, based on the temperature range chosen for the experiment. From the room-temperature measurements using thermocouples embedded inside the copper block the deviation was less than ±0.05°C. The total uncertainty of temperature differential was estimated to be ±5.4% at CHF and ±21.7% at minimum heat flux (MHF). Therefore, the total experimental uncertainties for the wall heat flux were estimated to be ±7.9% and ±28.5% at CHF and MHF points, respectively.

Experimental Results

A reference (control) experiment was performed using an atomically smooth bare silicon wafer. The effect of surface imperfections (e.g., cavities, grooves, etc.) on pool boiling was therefore eliminated using the bare silicon wafer. With commercial substrates (e.g., copper) the differences in distribution of the surface cavities on different substrates could make the boiling heat transfer data inconsistent for comparison. The control experiment therefore provides a consistent reference for the heat transfer augmentation due to presence of the different types of MWCNT. Also, by eliminating the effects of surface cavities—the complexities of the thermofluidic transport mechanisms are reduced. This helps to understand the physics of the boiling process on the MWCNT and to estimate the contribution to the total heat flux from the nano-structured surfaces compared to atomically smooth substrates.

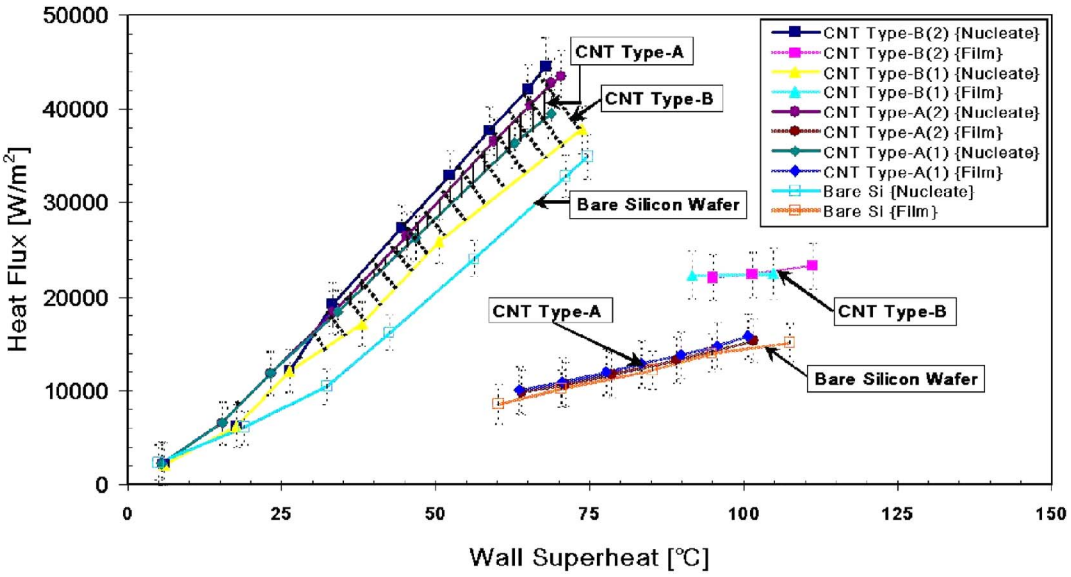

Fig. 5 Comparison of saturated pool boiling curve for PF-5060 on bare silicon and MWCNT synthesized on silicon. The MWCNT are of two different heights: type-A MWCNT (9 μm in height) and type-B MWCNT (25 μm in height). Saturation temperature of PF-5060=56°C (the numbers in parenthesis denote the experimental run).

Type-A MWCNT Forests (9 μm in height). Experiments were conducted for Type-A MWCNT forests deposited on a silicon wafer (height of MWCNT forests was 9 μm). Figure 3(*a*) shows the pool boiling curve obtained from experiments for the type-A MWCNT. No incipience excursion was observed in these experiments. The CHF point was obtained at wall superheat of 69°C, and the associated heat flux was 3.95×10^4 W/m^2. The experiment was repeated, and the CHF was obtained at wall superheat of 70°C with a heat flux value of 4.35×10^4 W/m^2.

On a bare silicon wafer, boiling inception was recorded at 3.2°C wall superheat (Fig. 3(*b*)). No incipience excursion was observed in these experiments. Critical heat flux (CHF) was achieved at 3.5×10^4 W/m^2 for a wall superheat of 75°C. The Leidenfrost point (MHF (minimum heat flux) in film boiling) was obtained at wall superheat of 60°C with an associated heat flux of 0.86×10^4 W/m^2. The difference in the wall superheat between the CHF and Leidenfrost points was ~15°C. The nucleate boiling heat fluxes are 25% lower than for type-A MWCNT.

In the film boiling regime, nearly identical heat flux values were obtained (within the bounds of the experimental uncertainty) for the two experimental runs with type-A MWCNT and bare silicon. The Leidenfrost point was found to occur at wall superheat of 64°C. The wall superheat at Leidenfrost point for type-A MWCNT forests is 4°C higher than that for bare silicon wafer. At the Leidenfrost point, the heat flux was 0.98×10^4 W/m^2, which is 14.4% higher than that for the bare silicon wafer. For type-A MWCNT forests, the difference in wall superheat between the CHF and Leidenfrost points is around 6°C (this is less than half of the corresponding difference for the bare silicon wafer).

Experiments Using Type-B MWCNT Forests (25 μm in height). Figure 4(*a*) shows the experimental results conducted with the type-B MWCNT forests deposited on a silicon wafer (height of MWCNT forests was 25 μm). As shown in Fig. 4, the heat flux values measured in nucleate boiling during the first experiment is smaller than the second experiment. On visual observation the MWCNT forests were found to contain two scratch marks, less than a centimeter long, on the edge of the wafer (possibly from the clamp) at the conclusion of the first experiment. However, on performing visual observation after the second experimental run, the MWCNT forests were found to be unaffected. For both experiments using type-B MWCNT, no incipience excursion was observed.

The heat fluxes in nucleate boiling for type-B MWCNT is less than that obtained for type-A MWCNT. However, the heat fluxes for type-B MWCNT are still higher than that for bare silicon wafer. The type-B MWCNT has lower heat flux at CHF point compared to type-A MWCNT, even though the wall super heat at CHF point is significantly higher than that for type-A MWCNT. The measured heat flux and the wall superheat at CHF point for type-B MWCNT were 3.79×10^4 W/m^2 and 74°C, respectively, for the first experimental run. The heat flux value and the associated wall superheat at CHF point were 4.46×10^4 W/m^2 and 68°C, respectively, for the second experimental run. This value of heat flux for type-B MWCNT is 28% higher than for bare silicon.

For the two trials with type-B MWCNT, CHF was obtained at 74°C and 68°C. On increasing the temperature beyond CHF conditions, a combination of nucleate and film boiling was observed. The film boiling region was localized near outer the edge of the

Table 2 Critical heat flux (CHF) and minimum heat flux (MHF) values for bare silicon, type-A MWCNT (9 μm), and type-B MWCNT (25 μm)

	Critical heat flux (CHF)		Minimum heat flux (MHF)	
	CHF$\times10^{-4}$ (W/m^2)	T_w-T_{sat}(°C)	MHF$\times10^{-4}$ (W/m^2)	T_w-T_{sat}(°C)
Bare Si	3.49	75	0.86	60
Type-A	4.35	70	0.98	64
Type-B	4.46	68	2.21	95

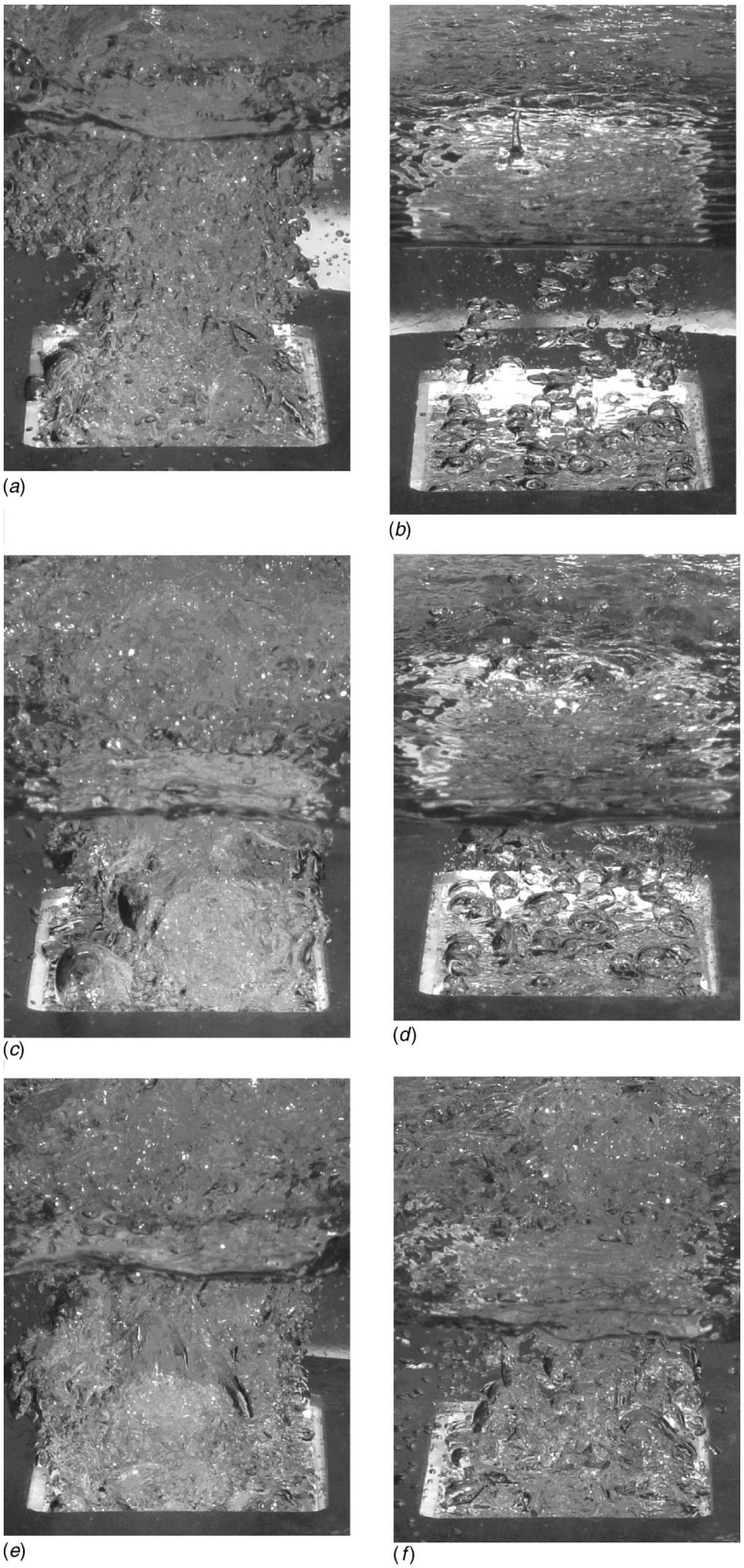

Fig. 6 Images of boiling obtained during the experiments: (*a*) near CHF point on bare silicon wafer, (*b*) near Leidenfrost point on bare silicon wafer, (*c*) near CHF point on type-A MWCNT, (*d*) near Leidenfrost point on type-A MWCNT, (*e*) near CHF point on type-B MWCNT, and (*f*) near Leidenfrost point on type-B MWCNT

silicon wafer (near the clamps), and the nucleate boiling region was localized in the center of the silicon wafer. This is characteristic of transition boiling regime. For wall superheats exceeding 105 °C, a continuous vapor film was observed over the whole area of the exposed wafer.

For film boiling regime, the heat flux for type-B MWCNT is higher than that for bare silicon. The heat flux measured near Leidenfrost point (at wall superheat of 95 °C) for type-B MWCNT was 2.21×10^4 W/m^2, which is 57% higher than that for bare silicon at the same wall superheat. Figure 4(*b*) shows a comparison of pool boiling curve for type-B MWCNT with bare silicon.

The effect of MWCNT forests (types A and B) on pool boiling is compared to that of the bare silicon wafer in Fig. 5. For nucleate boiling regime, type-A and type-B MWCNT forests have higher heat flux values than that for bare silicon at each of the data points for different wall superheat. The heat flux at CHF for type-A and type-B MWCNT are higher than for bare silicon. From the results, it can be concluded that the MWCNT enhances nucleate boiling heat flux, but the height of MWCNT is not a sensitive parameter.

For film boiling regime, the heat flux for type-B MWCNT is higher than that for type-A MWCNT and bare silicon. However, within the bounds of the experimental error - the heat flux values are almost identical for type-A MWCNT and the bare silicon wafer in the film boiling regime. The results show that the longer MWCNT enhances the film boiling performance and shifts Leidenfrost point to a higher superheat. The critical heat flux and minimum heat flux values are summarized in Table 2.

Figure 6 shows representative images of the various boiling regimes observed in the experiments. The images were obtained using Sony CyberShot DSC-P10 Digital Camera. As shown in the images obtained at CHF conditions in Fig. 6(*a*), 6(*c*), and 6(*e*), type-A and type-B MWCNT showed more vigorous ebullition of bubbles. For the images of film boiling at Leidenfrost point in Fig. 6(*b*), 6(*d*), and 6(*f*), the vapor film was clearly visible in the form of a shiny "mirror" type surface for bare silicon and type-A MWCNT. However, the area occupied by the shiny "mirror" type surface for type-B MWCNT was reduced in size and a larger proportion of the boiling area was covered with departing vapor bubbles. The images also show that the sizes of the departing bubbles are smaller, and there are larger numbers of bubble departure sites for type-B MWCNT (than type-A MWCNT or bare silicon). The images show that the vapor film was disrupted during film boiling over type-B MWCNT leading to formation of larger number of sites for bubble departure. Such disruptions of the vapor film were not observed for type-A MWCNT or bare silicon wafer, and consequently, the number of bubble departure sites was less compared to type-B MWCNT. Also, the bubble departure sites were observed to be more evenly spaced compared to type-B MWCNT. Figure 2 shows SEM images of the type-B MWCNT forests (using Zeiss 1530 VP FE-SEM at the Microscopy and Imaging Center at Texas A&M University) obtained before and after the boiling experiments were conducted. The SEM image in Fig. 2(*b*) was obtained before performing the boiling experiments and shows a network of threadlike MWCNT structures on the top surface. Figure 2(*c*) was obtained after performing the boiling experiments and at a higher magnification. The images show that the MWCNT are virtually identical before and after the experiments were conducted. This demonstrates that boiling experiments did not affect the inherent morphology of the MWCNT.

Discussion

The experimental results are consistent with numerical models reported in the literature. Earlier studies [7–9] predicted that the dynamic values of the minimum vapor film thickness in film boiling of PF-5060 are ~15–20 μm. The authors had discussed that surface roughness (or surface structures) greater than 10 μm could disrupt the vapor films leading to possible collapse of film boiling. It is observed that for type-B MWCNT (height of 25 μm) the film boiling heat flux is enhanced considerably compared to type-A MWCNT (height of 9 μm). This shows that MWCNT forests with heights greater than 10 μm possibly disrupt the vapor film.

The numerical study by Banerjee et al. [9] also demonstrated the existence of "cold spots" in film boiling. Cold spots are regions of lower surface temperature than the surrounding. The study [9] showed that cold spots serve as focused conduits for heat transfer in film boiling. The size of the cold spots was found to increase with the heater conductivity and resulted in higher average heat flux. Since MWCNT has higher thermal conductivity than the silicon substrate the efficacy of the cold spots in transferring heat is enhanced due to the presence of MWCNT. MWCNT structures that disrupt the vapor film at the minimum vapor film thickness (which is collocated with the cold spots) would further enhance transient heat transfer by inducing liquid-solid contacts. This is also expected to augment heat transfer by transient quenching of the surface. Hence, type-B MWCNT forests augment film boiling heat flux while for type-A MWCNT forests it is almost identical to bare silicon.

In contrast, the nucleate boiling heat flux is less sensitive to the height of MWCNT forests. Since the pitch of the MWCNT fibers are ~8–16 nm, it is expected that the nucleation mechanisms are considerably different compared to a conventional surface (where the size of nucleation cavities are typically ~5–10 μm dia). On nanostructured surfaces, the continuum models are not applicable since slip flow conditions would exist due to noncontinuum effects. The bubble nucleation potentially occurs on the exposed tip of the MWCNT. If the working liquid wets the MWCNT (e.g., PF-5060), it would penetrate the space between the nanotubes. For a poorly wetting liquid (e.g., for water on MWCNT), air or vapor layer can be trapped in the space between the nanotubes [14]. Inception of bubbles within the MWCNT is improbable due to the high superheats that are required for nucleation.

Conclusions

The results obtained from boiling experiments on vertically aligned multiwalled carbon nanotubes (MWCNT) of two different heights (type A: 9 μm and type B: 25 μm) are summarized as follows:

1. MWCNT forests are found to augment critical heat flux by ~25–28 % compared to control experiments.
2. Enhancement of nucleate boiling heat flux is not found to be sensitive to the height of the MWCNT forests.
3. In contrast, the film boiling heat flux is strongly sensitive to the height of the MWCNT forests. For type-B MWCNT (25 μm in height) the heat flux is enhanced by 57% compared to control experiments. However, for type-A MWCNT (9 μm in height) the heat flux values are similar to the control experiments. This is consistent with models for film boiling reported in the literature.
4. SEM images for the top view of the MWCNT structures obtained before and after the experiments show that the boiling experiments did not affect the inherent morphology of the MWCNT structures.

The mechanisms causing heat flux augmentation are identified as follows: (i) the high conductivity of MWCNT compared to the silicon substrate resulting in higher sensible heat transfer (conduction and convection); (ii) larger sized cold spots leading to higher average heat flux; (iii) vapor film collapse caused by MWCNT; (iv) enhanced liquid-solid contacts resulting in transient quenching of the surface; and (v) the enhanced surface areas resulting from the presence of MWCNT in the form of "nanofins."

Acknowledgment

The authors gratefully acknowledge support from the Texas Engineering Experimentation Station and the Mechanical Engineering Department. Access to laboratory facilities by Dr. S. Lau at Texas A&M is gratefully acknowledged. FE-SEM acquisition was supported by the National Science Foundation (Grant No. DBI-0116835).

Nomenclature

A_w = wall area on which boiling occurs
R_t = Thermal resistance
T = temperature
k = thermal conductivity
q'' = heat flux
x = distance

Greek symbols

Δ = difference
ω = uncertainty

Subscripts

c = top surface of copper block
sat = saturation
w = wall of a silicon wafer (at boiling side)

References

[1] Ramaswamy, C., Joshi, Y. K., Nakayama, W., and Johnson, W. B., 2000, "Combined Effects of Sub-cooling and Operating Pressure on the Performance of a Two-Chamber Thermo-Siphon," IEEE Trans. Compon. Packag. Technol., **23**(1), pp. 61–69.

[2] Mudawar, I., and Anderson, T. M., 1993, "Optimization of Enhanced Surfaces for High Flux Chip Cooling by Pool Boiling," ASME J. Electron. Packag., **115**, pp. 89–100.

[3] Coursey, J. S., Roh, H., Kim, J., and Boudreaux, P. J., 2002, "Graphite Foam Thermosyphon Evaporator Performance: Parametric Investigation of the Effects of Working Fluid, Liquid Level, and Chamber Pressure," *Proceeding of the ASME IMECE 2002*, New Orleans, LA, Paper No. 2002-33733.

[4] Iijima, S., 1991, "Helical Microtubules of Graphitic Carbon," Nature (London), **354**, pp. 56–58.

[5] Berber, S., Kwon, Y. K., and Tomanek, D., 2000, "Unusually High Thermal Conductivity of Carbon Nanotubes," Phys. Rev. Lett., **84**, pp. 4613–4616.

[6] Banerjee, D., 1999, "Numerical and Experimental Investigation of Subcooled Film Boiling on a Horizontal Plate," Ph.D. thesis, University of California, Los Angeles.

[7] Banerjee, D., and Dhir, V. K., 2001, "Study of Subcooled Film Boiling on a Horizontal Disc, Part 1: Analysis," ASME J. Heat Transfer, **123**, pp. 271–284.

[8] Banerjee, D., and Dhir, V. K., 2001, "Study of Subcooled Film Boiling on a Horizontal Disc, Part 2: Experiments," ASME J. Heat Transfer, **123**, pp. 285–293.

[9] Banerjee, D., Son, G., and Dhir, V. K., 1996, "Conjugate Thermal and Hydrodynamic Analysis of Saturated Film Boiling From a Horizontal Surface," ASME HTD, 334, Part 3, pp. 57–64.

[10] Zhang, M., Fang, S., Zakhidov, A. A., Lee, S. B., Aliev, A. E., Williams, C. D., Atkinson, K. R., and Baughman, R., 2005, "Strong, Transparent, Multifunctional, Carbon Nanotube Sheets," Science, **309**, pp. 1215–1219.

[11] Ahn, H. S., Sinha, N., and Banerjee, D., 2005, "Micromachined Temperature Sensor Arrays for Studying Micro-scale Features in Film Boiling," *Proceedings of the ASME-IMECE 2005*, Orlando, Nov. 5–11, ASME.

[12] Kline, S. J., and McClintock, F. A., 1953, "Describing the Uncertainties in Single Sample Experiments," Mech. Eng. (Am. Soc. Mech. Eng.), **75**, pp. 3–8.

[13] Mills, A. F., 1999, *Heat Transfer*, 2nd ed., Prentice-Hall, Englewood Cliffs, NJ.

[14] Krupenkin, T. N., Taylor, J. A., Schneider, T. M., and Yang, S., 2004, "From Rolling Ball to Complete Wetting: The Dynamic Tuning of Liquids on Nanostructured Surfaces," Langmuir, **20**(10), pp. 3824–3827.